

Homogenization of fault frictional properties

Sohom Ray¹ and Robert C. Viesca¹

¹ Tufts University, Medford, MA-02155

Received 2019 April 15; in original form 2019 April 15

SUMMARY

The frictional properties of large faults are expected to vary in space. However, fault models often assume properties are homogeneous, or nearly so. We investigate the conditions under which the details of variations may be neglected and properties homogenized. We do so by examining the behavior of nonlinear solutions for unstably accelerating fault slip under frictional heterogeneity. We consider a rate- and state-dependent fault friction, in which the characteristic wavelength for the property variations is a problem parameter. We find that homogenization is permissible only when that wavelength shows scale separation from an elasto-frictional length scale. However, fault models also often include property transitions that occur over distances comparable to the elasto-frictional length. We show that under such comparable variations, the dynamics of earthquake-nucleating instabilities are controlled by the properties' spatial distribution.

Key words: Earthquake Nucleation; Landslides; Rate-and-state friction; Slip instabilities; Blow-up solutions; Heterogeneities; Bifurcations; Stability Analysis; Homogenization; Hilbert transform.

1 INTRODUCTION

This study assesses the quasi-static evolution of fault slip considering fault's frictional properties to be nonuniformly distributed over a wide range of lengthscales. We consider slip rate and state dependence of fault shear strength and that the parameters in its constitutive formulation (a , b , σ and D_c) are functions of position on the fault. Previous studies with homogeneous fault frictional properties showed that blow-up solutions exist for slip rate instabilities on fault (e.g., Rubin et al., 1999; Viesca, 2016a,b). Subsequently, Ray & Viesca (2017) found that a finite number of multiple blow-up solutions exist when fault frictional properties are nonuniform. Here we consider variations of frictional parameters over a characteristic wavelength and examine how the size of that wavelength influences the blow-up solutions as well as their stability.

Following laboratory rock friction studies (e.g., Stesky, 1975; Dieterich, 1981; Blanpied et al., 1991) fault frictional properties at depth have been thought to be vary with depth and this variation has been reflected in seismic cycle models (e.g., Tse & Rice, 1986). Often, simple representations of these variations on mature faults are chosen: homogeneity over large intervals with transitions occurring further down dip. However, several observations indicate that frictional heterogeneity may exist over large regions of a fault at various scales, observations such as the clustering of microseismicity (e.g., Rubin & Ampuero, 2005; Waldhauser et al., 2004). This raises questions as to what extent can homogeneity be taken in place of considering detailed distribution of properties. Specifically, is it possible to lose important information by using averages of variable quantities. In other words, can homogenizing be ingenuous? How does the presence or absence of homogeneity affect the dynamics of models of seismic cycles?

Past studies of the influence of heterogeneity on fault rupture have focused on rate-independent descriptions of fault strength, as implied by a slip-dependent strength or the assumption of a constant fracture energy. Such descriptions lend themselves to application of concepts from classical, linear-elastic fracture mechanics, in which knowledge of the spatial distribution of stress or strength is used to make predictions regarding rupture propagation and arrest. For example, fault stress may be presumed to vary in space, while properties determining frictional strength are taken to be uniform, such as in the determination of rupture extent in numerical simulations or in experimental, laboratory ruptures Ampuero et al. (2006); Ripperger et al. (2007); Kammer et al. (2015); Bayart et al. (2015); Ke et al. (2018). In the former, the stress field is known such that rupture extent can be predicted *a priori*, and in the latter rupture extent is predicted retrospectively using measurements of stress changes following rupture. While in both examples, the so-called fracture energy of the fault is typically presumed a material constant, there has also been an interest in understanding how variations of the fault fracture energy, by way of varying frictional properties, affect the statistics of rupture events (e.g., Aochi & Ide, 2004).

2 Sohom Ray

However, laboratory and theoretical studies indicate that fault strength has a rate-dependence, in manners such that the fracture energy may not be considered to be a local property of the fault. The dependence may be weak at interseismic slip rates (Ruina, 1983, e.g.) or strong for mechanisms thought to operate during fast, co-seismic slip (e.g., Rice, 2006; Goldsby & Tullis, 2011). This rate dependence, however, raises difficulties in the analysis of spatial variations of frictional properties. Here we focus on the problem of earthquake nucleation to begin to address the above questions. Specifically, we consider a slip rate- and state-dependent fault friction and we examine instability development on faults with spatial distributions of frictional parameters. Prior work has considered the emergence of earthquake-nucleating instabilities on faults with spatially uniform properties using both linear Rice & Ruina (1983); Rice et al. (2001); Aldam et al. (2017) and nonlinear Dieterich (1992); Rubin & Ampuero (2005); Viesca (2016a,b) analysis and numerical solutions. Using previous analysis of instability under heterogeneous frictional properties (Ray & Viesca, 2017) and in the light of recent developments on heterogeneous faults (Dublanchet, 2017; Luo & Liu, 2019), we seek to determine the role of the length scale over which properties transition.

2 EQUATIONS GOVERNING QUASI-STATIC FAULT SLIP

2.1 Fault shear traction

We consider a geological fault as an interface, within a continuum, that accommodates relative motion. The fault is presumed to be located along $x - z$ plane containing the origin; and we consider in- or anti-plane deformation in which the magnitude of the displacement varies only over x . The ambient stress and displacement fields in the medium are identified respectively as $\sigma_{ij}(x, y, t)$ and $u_i(x, y, t)$. On the fault, the magnitude of the displacement discontinuity is referred to as slip, which is considered to vary only along x and is given by $\delta(x, t) = u_i(x, 0^+, t) - u_i(x, 0^-, t)$, where $i = x$ or z denote in-plane (mode II) or anti-plane (mode III) shearing respectively.

In absence of any differential slip along the fault, the shear traction on the fault surface is purely due to any remote loading, which resolves onto the fault surface as τ_{ex} . When the fault accommodates slip, the fault shear traction changes by an amount τ_{el} , due to the elastic deformation of the fault bounding medium. The total fault shear traction τ due to the medium's loading and response to nonuniform slip is then, given by,

$$\tau(x, t) = \tau_{ex}(x, t) + \tau_{el}(x, t) \quad (1)$$

We consider here slow, quasistatic deformation in which τ_{el} is determined by the current distribution of the slip $\delta(x, t)$. For in- or anti-plane slip on an unbounded fault between two elastic half spaces

$$\tau_{el}(x, t) = \frac{\bar{\mu}}{2\pi} \int_{-\infty}^{\infty} \frac{\partial \delta(\xi, t)/\partial \xi}{\xi - x} d\xi \quad (2)$$

where $\bar{\mu} := \mu/(1 - \nu)$ and $\bar{\mu} := \mu$ for in- and anti-plane slip, respectively (e.g., Bilby & Eshelby, 1968; Rice, 1968). For a fault lying below and parallel to a free surface a distance h away, τ_{el} is more simply expressed as

$$\tau_{el}(x, t) = \bar{E}h \frac{\partial^2 \delta(x, t)}{\partial x^2} \quad (3)$$

provided that variations in slip $\delta(x, t)$ occur over distances much larger than h [supplementary materials, Viesca (2016b)], where the elastic modulus $\bar{E} := 2\mu/(1 - \nu)$ and $\bar{E} := \mu$ for mode-II and mode-III sliding respectively. μ and ν are the shear modulus and Poisson's ratio, respectively.

Such a so-called thin slab configuration has been presumed to well represent the elastic deformation of translational landslides and ice sheets in response to basal slip (e.g., Puzrin & Germanovich, 2005; Lipovsky & Dunham, 2017), and also as a more mathematically convenient representation of elastic interactions between points on a fault (e.g., Bar-Sinai et al., 2012). As discussed in Viesca (2016a,b) and Ray & Viesca (2017), the two models, while representing two end-members of elastic interactions, long- and short-ranged, can give rise to qualitatively similar behavior. In the sections to follow, we present results for the thin-slab fault-model, though the results are generally qualitatively similar to the elastic configuration.

2.2 Fault frictional strength

We presume the fault shear strength, τ_s , is purely frictional and given by

$$\tau_s(x, t) = \sigma(x, t)f(x, t) \quad (4)$$

where σ is the fault-normal stress and f is the friction coefficient. In the case of a fluid-saturated fault zone, σ is the effective fault-normal stress, $\sigma(x, t) = \sigma_n(x, t) - p(x, t)$, where $\sigma_n(x, t)$ is the total normal stress and $p(x, t)$ is the pore fluid pressure. We consider a rate- and state-dependent formulation Dieterich (1978); Ruina (1983) in which f is a function of the instantaneous rate of slip $V(x, t) = \partial \delta / \partial t$, a state variable $\theta(x, t)$, and heterogeneous material parameters $a(x)$ and $b(x)$ at that position

$$f(x, t) = f_o + a(x) \ln \left[\frac{V(x, t)}{V_o} \right] + b(x) \ln \left[\frac{\theta(x, t)}{\theta_o} \right] \quad (5)$$

We consider, the aging-law evolution of state Ruina (1983), in which,

$$\frac{\partial \theta}{\partial t} = 1 - \frac{V(x, t)\theta(x, t)}{D_c(x)}. \quad (6)$$

Here, $D_c(x)$ is the characteristic slip over which friction evolves which we also allow to vary along the fault. The formulation exhibits the logarithmic rate dependence for steady-state sliding ($\partial\theta/\partial t = 0$) as shown below.

$$f_{ss}(x, t) = f_o + [a(x) - b(x)] \ln \left[\frac{V(x, t)}{V_o} \right]$$

In (5) and above, f_o is the reference coefficient of friction at steady sliding velocity V_o and state $\theta_o = D_c/V_o$. Fault surfaces with $a < b$ are potentially destabilizing because an increase in sliding rate subsequently leads to a weakened new steady-state shear strength. Such steady-state rate-weakening surfaces, when subjected to stress or velocity perturbations can lead to an instability that might nucleate an earthquake generating dynamic rupture (e.g., Rice & Ruina, 1983)

Considering the form of slip acceleration (Appendix A) motivates us to choose an alternate state variable $\Phi(x, t)$ given by

$$\Phi(x, t) := -\frac{D_c(x)}{V(x, t)} \frac{\partial \theta}{\partial t} \quad (7)$$

which for the aging law of state evolution assumes the form

$$\Phi(x, t) = 1 - \frac{D_c(x)}{V(x, t)\theta(x, t)}. \quad (8)$$

With this definition, $\Phi(x, t)$ can be interpreted as a convenient measure for nearness of fault slip to steady-state sliding: $\Phi = 0$ occurs for steady state sliding and $\Phi = 1$ when the state of the slip is far from steady state.

2.3 Slip rate and state evolution equations

Frictional resistance requires that when and where slip rate is nonzero the total shear stress is equal to the strength of the fault $\tau(x, t) = \tau_s(x, t)$. Evolution equations for slip rate and the alternate state variable Φ follow from the equations in Section 2 and are expressible in the form

$$\frac{\partial V}{\partial t} = \mathcal{R}[V(x, t), \Phi(x, t)] \quad (9a)$$

$$\frac{\partial \Phi}{\partial t} = \mathcal{S}[V(x, t), \Phi(x, t)] \quad (9b)$$

where the operators \mathcal{R} and \mathcal{S} depend on the elastic configuration, the distribution of $a(x)$, $b(x)$ and $D_c(x)$, and also on the external stress-rate (Appendix A), though we have dropped explicit reference to these latter terms here.

The interaction between the elasticity of the bounding medium and the frictional strength of the interface defines an elasto-frictional length scale for strength and slip variations along the interface. For an interface lying within a full-space, such a length scale is $L_b = \bar{\mu}D_c/b\sigma$ Dieterich (1992); Rubin & Ampuero (2005), when the evolution-effect parameter b is uniform. Likewise, for the thin-slab configurations, a length scale is $L_{bh} = \sqrt{\bar{E}hD_c/b\sigma}$ Viesca (2016a,b). When a or b vary, we may use instead $L_n = \bar{\mu}D_c/\sigma$ and $L_{nh} = \sqrt{\bar{E}hD_c/\sigma}$, for the and thin-slab configurations, respectively Ray & Viesca (2017).

3 FINITE-TIME INSTABILITY OF SLIP RATE

Prior work showed the existence of solutions in which slip rate quasi-statically diverges within finite time on faults with heterogeneous frictional parameters Ray & Viesca (2017). Specifically, the solutions have the form

$$V(x, t) = \frac{D_c(x)}{t_f(t)} \mathcal{W}(x) \quad (10)$$

where $t_f(t) = t_{in} - t$, t_{in} is the finite time of the instability, and the spatial distribution $\mathcal{W}(x)$ is to be solved for and depends on the distribution of the parameters a, b , as well as the normal stress distribution at times approaching t_{in} .

In addition to showing the existence of (10), Ray & Viesca (2017) also determined whether these types of solutions would likely represent how slip rate would locally, quasi-statically diverge in the moments preceding dynamic rupture in a model with rate- and state-dependent friction. Following Viesca (2016a,b), this was done in treating the distribution $\mathcal{W}(x)$ as a fixed point of a dynamical system and assessing its stability. The analysis reduces to determining whether perturbations to the diverging slip rate (10) themselves diverge or decay as $t_f \rightarrow 0$. We look for perturbations of the form Barenblatt (1996)

$$V(x, t) = \frac{D_c(x)}{t_f} \left[\mathcal{W}(x) + \omega(x)(t_f/t_o)^{-\lambda} \right] \quad (11)$$

where t_o is an arbitrary timescale; and the distribution $\omega(x)$ and constant λ are to be determined and reduce to eigenfunctions and eigenvalues, respectively, of an eigenvalue problem, described in Ray & Viesca (2017). The stability of the blow-up solutions is determined by the

4 Sohom Ray

eigenvalue λ with a largest real part (other than the symmetry modes). We distinguish that eigenvalue using the notation λ_{max} . If a mode exists with $\text{Re}(\lambda_{max}) > 0$, then the solution (10) is said to be unstable, and the solution is stable in the absence of such a mode.

In Appendix B2, we note that eigenvalues $\lambda = 0$ and $\lambda = 1$ —with respective eigenfunctions $\mathcal{W}'(x)$ and $\mathcal{W}(x)$ —correspond to, respectively, spatial and temporal translational symmetry of the problem: they have no bearing on the stability of the blow-up solutions (e.g., Viesca, 2016b; Ray & Viesca, 2017). Temporal symmetry exists for all problem parameters, and, consequently, the temporal symmetry mode ($\lambda = 1$ and $\omega(x) = \mathcal{W}(x)$) appears in the stability analysis of the solutions. However, the spatial symmetry mode ($\lambda = 0$ and $\omega(x) = \mathcal{W}'(x)$) appears when all the problem parameters remain uniform in space.

4 ASSESSING THE INFLUENCE OF FAULT HETEROGENEITY ON EARTHQUAKE NUCLEATION

The stability analysis of solutions (10) is particularly significant when fault frictional properties are nonuniformly distributed. Considering a fault with dimension large compared to the nucleation length and with properties homogeneous, an invariance exists with respect to translations in space except within nucleation length from fault boundaries; and, in turn, a solution of the type (10) exist about any point on the fault sufficiently away from the boundaries. Solution of the type (10) exists close to the boundaries; however, not spatially translatable owed to the lost spatial invariance. In contrast to the homogenous conditions, for a fault with heterogeneous properties, there are a finite number of blow-up solutions (10) distributed at critical points on the fault. Only a subset of these solutions are stable; and, in turn, only those associated critical points on the fault can be expected to nucleate a dynamic rupture (Ray & Viesca, 2017).

However, an important question remains: how does the rate at which properties vary along the fault affect the existence of solutions (10), as well as their stability? A related question of particular interest is whether, and under what conditions, may frictional properties be effectively homogenized. Rather than considering the variations of parameters a or b individually, we focus on variations of the magnitude of steady-state rate-weakening, as well as a measure of its relative magnitude, defined respectively as

$$m(x) := b(x) - a(x)$$

$$r(x) := \frac{b(x) - a(x)}{b(x)}$$

We consider simple forms for their along-fault variations on fault

$$m(x) = m_o + m_1 \cos(\kappa x / L_{ef}) \quad (12a)$$

$$r(x) = r_o + r_1 \cos(\kappa x / L_{ef}) \quad (12b)$$

where κ is a dimensionless wavenumber and L_{ef} is an elasto-frictional length, which is a placeholder for L_{nh} or L_{bh} , depending on whether b varies or not, respectively, in arriving to the distributions (B.5). The dimensionless wavelength, $2\pi\kappa^{-1}$, measures the lengthscale of property variation against the elasto-frictional length. We now analyze how κ affects the blow-up solutions and their stability.

5 RESULTS

We highlight blow-up solutions and their stability results for three particular cases in Fig. 1: a case of homogeneously distributed parameters (Fig. 1a), and two heterogeneous cases with an increasing degree of heterogeneity, i.e., an increase in the wavenumber κ (Fig. 1b,c). In the homogeneous case, there is one solution for the distribution $\mathcal{W}(x)$ (Fig. 1d) that may be spatially translated. An analysis of its stability shows that it is a stable, attractive solution. Specifically, there are only two modes with $\text{Re}(\lambda_{max}) \geq 0$: these are associated spatial and temporal translational invariance (Fig. 1g, dashed and solid lines, respectively) and do not influence solution stability (e.g., Viesca, 2016b; Ray & Viesca, 2017). Introducing some heterogeneity (Fig. 1b), spatial translational invariance no longer exists, and we find that a blow-up solutions are confined to extrema in the distribution (Fig. 1e). In this case the solution at the maximum of r is stable, at that at the minimum is unstable. A stability analysis of the former shows no modes with $\text{Re}(\lambda_{max}) > 0$, apart from the temporal invariance mode (Fig. 1h, solid black curve). A stability analysis of the latter shows an unstable mode (Fig. 1i, red curve), in addition to the translational mode (Fig. 1i, black curve). Considering a heterogeneous case with increased κ (Fig. 1c), we find that the solutions are still confined to extrema (Fig. 1f, in which solutions for only two extrema are shown). However, we now find that the stability of the solutions at the extrema are reversed from the case of Fig. 1b: the solutions at the maxima are unstable and those at minima are stable (Fig. 1j,k). This stability implies that the regions with the lowest magnitude of steady-state rate-weakening are now the attractive location for instability.

The remarkable reversal of stability with decreasing wavelength of property variations is reflected in numerical solutions for the evolution of slip rate (Fig. 2). Beginning with initially steady-state conditions, we introduce at $t = 0$ a locally peaked stressing rate centered at a position between a maximum and minimum in the distribution of r . An unstable acceleration of slip follows and we plot in Fig. 2b the slip rate, scaled by its maximum value at snapshots in time. As time progresses, the slip rate diverges and approaches the expected distribution of the stable blow-up solution (green dashed line, Fig. 2b). In Fig. 2c, we increase κ to the point where the stability is reversed. This reversal is reflected in the evolution of the diverging slip rate (Fig. 2d).

To better understand the reversal of stability as κ changes, we examined its influence on λ_{max} , defined as the maximum eigenvalue associated with the blow-up solutions at the peak and troughs of the distributions (Figs. 3 and 4a). As before, when $\text{Re}(\lambda_{max}) > 0$, the

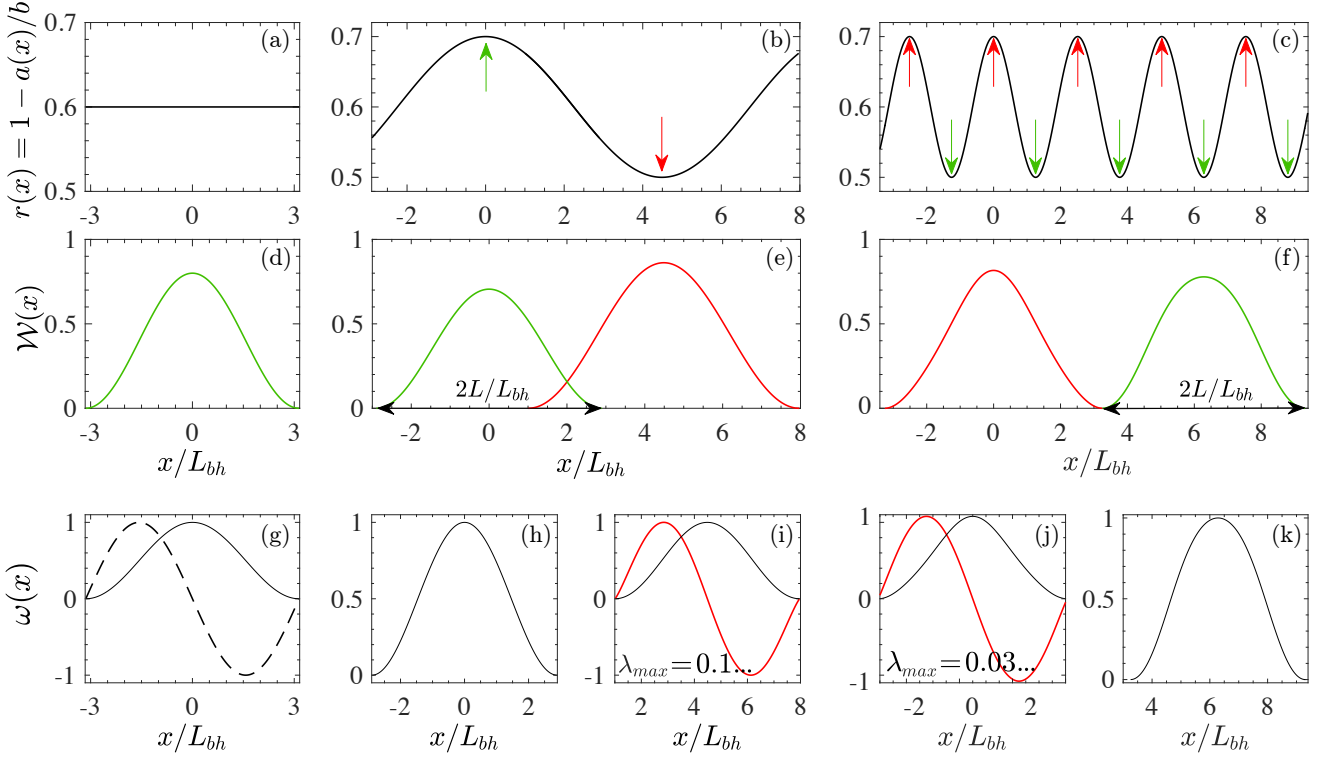


Figure 1. Fixed point solutions and their stability under different wavelengths of frictional property variation. Plots, along the fault length x , of (a–c) the variation of $r = 1 - a/b$; (d–f) stable (green) and unstable (red) blow-up solutions (10) corresponding to the overlying distributions; and (g–k) eigenmodes including temporal (black) and spatial (dashed) symmetry modes, and unstable modes (red) with $\text{Re}(\lambda_{\max}) > 0$. Panels in rows (d–f) and (g–k) correspond to the property variations (a–c) at the top of the panel columns. Introduction of heterogeneity restricts blow-up solutions to frictional property extrema. Only a subset of these solutions are stable and increasing the degree of heterogeneity leads to reversals in stability.

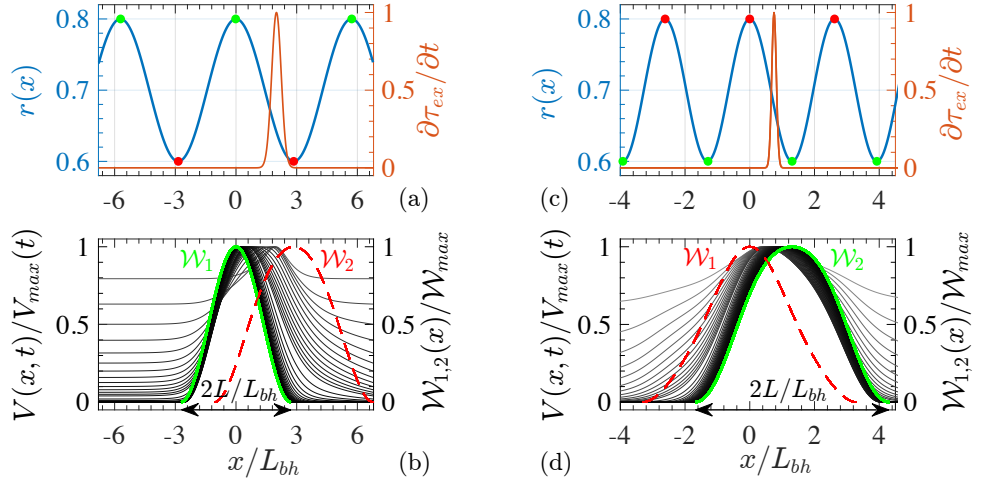


Figure 2. Decreasing the wavelength of frictional property variations leads to a reversal in which fault locations are attractive for instability development. (a,c) Distributions $r(x) = 1 - a(x)/b$ along fault position x (blue) with two different wavelengths and location of a local, constant stressing rate (red). Green (red) dots highlight locations of stable (unstable) blow-up solutions. (b,d) Numerical solutions for slip rate evolution for a fault subject to the local stressing for distributions (a) and (c), respectively. Slip rate shown at instants in time, scaled by the maximum value at each time (greyscale) and blow-up solutions scaled by peak values (red, green). Green and red curves correspond to stable and unstable solutions.

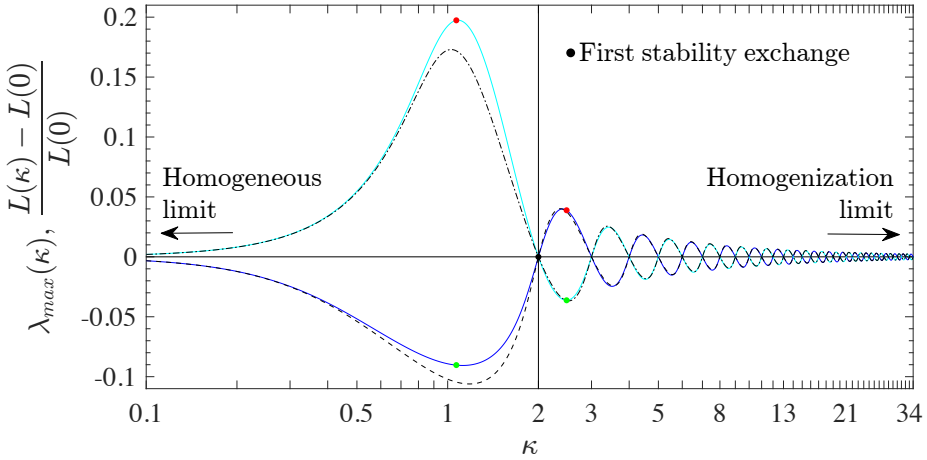


Figure 3. Exchange of stability of blow-up solutions occurring about the maxima and minima of a distribution of a frictional property distribution. The absolute m and relative rate weakening r vary in phase with $r(x) = 0.6 + 0.1 \cos(\kappa x/L_{bh})$, similarly to Fig. 2. We solve for the stability of blow-up solutions as a function of the wavenumber κ . We show the maximum eigenvalue λ_{max} for blow-up solutions occurring about the maxima (blue) and minima (cyan) of the distribution of r . Solutions are unstable if $\lambda_{max} > 0$ and stable otherwise. Colored dots correspond to cases examined in Fig. 2. Stability exchanges occur at integer values of κ . Also shown are the corresponding values for the nucleation half-length L for blow-up solutions at maxima (dashed) and minima (dash-dotted), relative to its value in the homogeneous limit $L(\kappa = 0) = \pi L_{bh}$.

blow-up solution is unstable, and stable otherwise. We consider two elementary scenarios: both $r(x)$ and $m(x)$ vary in phase, as may occur if a varies and b is held fixed (Fig. 3); or a variable $m(x)$ under a constant and uniform r (Fig. 4). In each case, the blow-up solutions are found to exist only at critical regions: about the extrema of parameter distributions, and, in some cases, between them. In Figs. 3 and 4a, the cyan and blue curves are indicator of the stability of the blow-up solutions at the minimum and maximum of the parameter variations, respectively. In Fig. 4a, the magenta-colored curve corresponds to the stability of the blow-up solutions that occur around the inflection points of $m(x)$ when wavenumber κ is within the red-colored regime. In the following sub-sections, we comment on the behavior at long, intermediate, and short wavelengths of parameter variations. We make a brief aside to discuss what is meant by long (or short) wavelengths. We recall that we have scaled wavelengths and wavenumber by an elasto-frictional length, such that, for example, the interpretation of small κ is that wavelengths are large in comparison to this length. However, we also recall that another relevant length exists: the nucleation length denoted by L , which is the half-length of the region for the distribution \mathcal{W} (e.g., illustrated in Figs. 1 and 2). In the homogeneous limit for the cases studied here, in which $a/b = 0.5$, L is comparable to the elasto-frictional length: $L = \pi L_{bh}$ Viesca (2016b). Thus, a distinction does not need to be explicitly made in our discussions above and to follow. However, we must note that, for homogeneous properties, as $a/b \rightarrow 1$, L generally diverges in comparison with the elasto-frictional lengthscales used here (L_b or L_{bh}) Viesca (2016a,b). In this limit, careful attention must be paid to the relevant lengthscale with which to compare distances over which frictional properties vary. The most relevant length is L , the length over which solutions (10) sample property variations. While L is not known a priori for arbitrary property variations, L is known for homogeneous frictional properties (Rubin & Ampuero, 2005; Viesca, 2016a,b), which provides a first estimate using averaged quantities for heterogeneous faults. Apart from the elasto-frictional length scale, L is dependent on the ratio a/b . For the half-space and thin-slab configurations, respectively, $L = L_b/[\pi(1-a/b)^2]$ and $L = L_{bh}/(1-a/b)$ in the limit $a/b \rightarrow 1$ Viesca (2016a,b).

5.1 Long and intermediate wavelengths

With variations over long wavelengths ($\kappa \ll 1$), we find that whether the local maxima or minima of frictional properties are the locations of attractive blow-up depends on what frictional properties vary. In Fig. 3, in which m and r both vary in phase, blow-up solutions about the local maxima are stable and those about the minima are unstable (as in Fig. 2a,b). To contrast, in Fig. 4a, we find that under fixed r and variable m , it is the minima of m that are attractive locations for instability.

At small values of κ , we also find a third possibility for instability progression when r is fixed and m varies: blow-up of slip rate at a region between the maximum and minimum. As alluded to above, this third possibility occurs transiently as κ increases: first appearing close to $\kappa = 0.2$ and disappearing close to $\kappa = 0.35$ (red areas in Fig. 4). Its corresponding value of λ_{max} is shown in magenta in Fig. 4a. The appearance of these intervening solutions coincides with the loss of stability of blow-up solutions occurring about the minima of m , and their disappearance coincides with the return of stability of the solutions occurring about the maxima. In Fig. 4b we illustrate the abrupt appearance of these intervening blow-up solutions. At $\kappa = 0.15$ we show the solution for $\mathcal{W}(x)$ that occurs about a maximum. Additional solutions for $\mathcal{W}(x)$ suddenly appear in the region between the maximum and adjacent minima around $\kappa = 0.2$ and are stable. As κ increases further, the position of these attractive intervening solutions approaches the solution at the maximum. Ultimately, the intervening solutions collide with that at the maximum around $\kappa = 0.35$. At this point, the latter solution remains and regains stability.

Intermediate values of κ mark a qualitative transition in stability behavior of the blow-up solutions. As κ increases from small

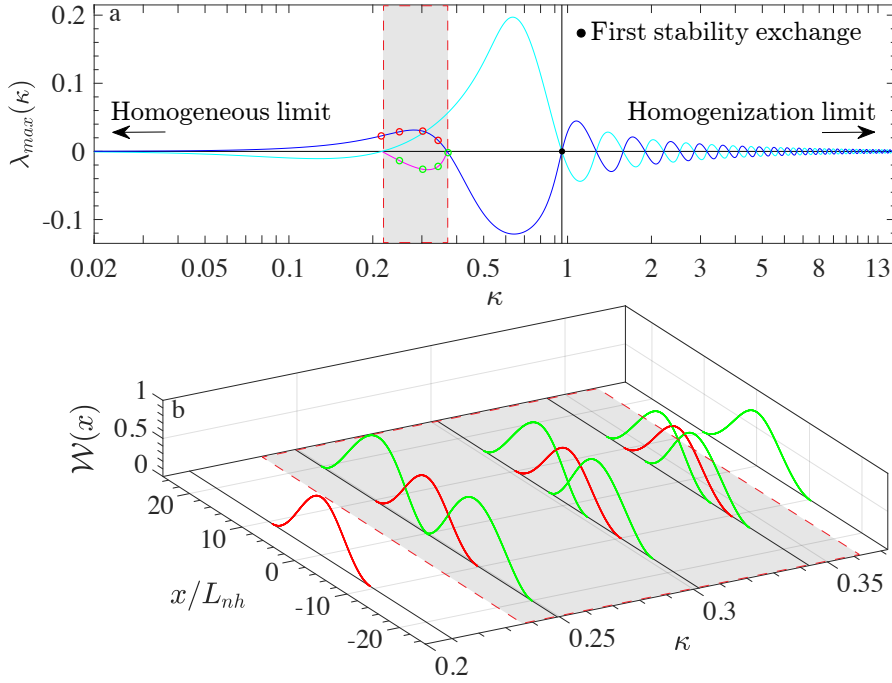


Figure 4. Under fixed $r = 1 - a/b$ and variable $m = b - a$, an exchange of stability occurs similarly to that in Fig. 3, except with additional bifurcations at small values of κ (red region). Here $m(x) = 0.06 + 0.02 \cos(\kappa x/L_{nh})$ with a constant $r = 0.6$. (a) Plot of the maximum eigenvalue λ_{max} as a function κ from the stability analysis of blow-up solutions at maxima (blue) and minima (cyan) of $m(x)$. λ_{max} for a third type of blow-up solution, which appears in the region between extrema, is shown in magenta. (b) Illustration of the sudden appearance and disappearance of the third-type of blow-up solution (see text for description). The green and red dots in (a) correspond to the solutions of the same colors in (b); these colors correspond to stable (attractive) or unstable (unattractive) blow-up solutions.

values, λ_{max} takes on its most positive and negative values close to $\kappa = 1$ for the two cases. Subsequently, an exchange of stability of the solutions at the maxima and minima occurs. It is this exchange of stability that is captured in Fig 2. This exchange of stability repeats indefinitely as κ increases.

In Fig. 3 we show the value of the nucleation half-length L for solutions at both extrema (dashed and dash-dotted lines). L is shown as a relative change from its value under homogeneous frictional properties ($\kappa = 0$), for which $L = \pi L_{bh}$ Viesca (2016b). At long wavelengths, there is a small departure from the homogeneous value, which matches the asymptotic behavior of λ_{max} . The departure remains modest (<20%) at intermediate wavelengths, and returns to zero precisely when the exchange of stability occurs.

5.2 Short wavelengths and homogenization

Remarkably, the behavior at large κ , at which the frictional properties are highly heterogeneous, is that of a homogeneous fault with the spatially averaged values of the variable properties. Specifically, the blow-up solutions at the extrema converge to the spatially translatable solution under homogeneous conditions for the average value of $a/b = 0.4$. As $\kappa \rightarrow \infty$, $\mathcal{W}(x)$ at both the maxima and minima converge towards the homogeneous solution, in which $L = \pi L_{bh}$ and, to within a spatial translation, $\mathcal{W}(x) = [1 + \cos(x/L_{bh})]/2$, where $L = \pi L_{bh}$ Viesca (2016b). Simultaneously in this limit, λ_{max} and the corresponding eigenmode $\omega(x)$ asymptotically approach the expected values for a translational symmetry mode: $\lambda = 0$ and $\omega(x) = \mathcal{W}'(x) = -\sin(x/L_{bh})$ Viesca (2016b). That a translational invariance re-emerges is the consequence of the maxima and minima being separated over distances much smaller than the nucleation length L as $\kappa \rightarrow \infty$. The convergence of L and λ_{max} for the case of variable r and m is shown in Fig. 3, and the convergence of λ_{max} for the case of fixed r and variable m is shown in 4. During the convergence, there is an exchange of stability between the solutions at maxima and minima, with an ever-decreasing amplitude for the eigenvalue λ_{max} for each solution. For the case of variable r and m , the stability exchange occurs at integer values of κ (Appendix C).

6 CONCLUSION

We show that homogenization of frictional parameters for slip rate- and state-dependent friction is justifiable in the limits of variations occurring over relatively long or short lengthscales. In the former case, frictional parameters vary gradually relative to spatial variations in slip rate, which scale with the elasto-frictional length. The evolution of slip rate is expected to follow that of a homogeneous fault with the

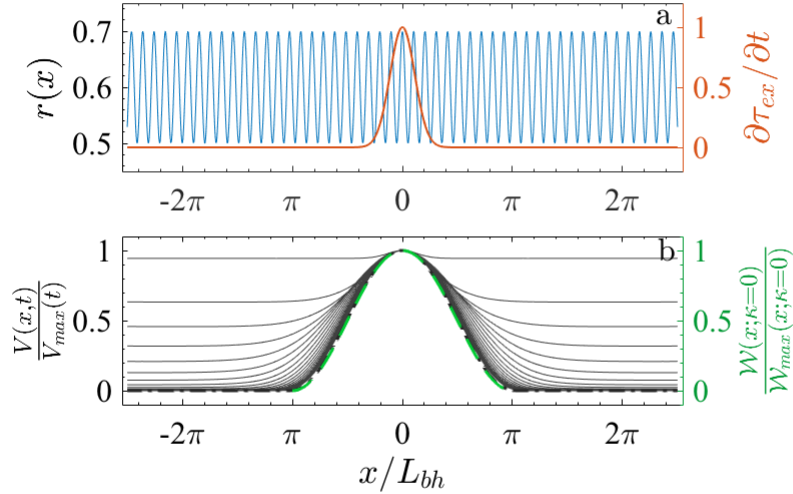


Figure 5. Results of evolution of slip rate under high degree of fault frictional heterogeneity is compared against the fixed point solution for homogenous case. (a) A variable $r(x) = 0.6 + 0.1 \cos(\kappa x / L_{bh})$ with $\kappa = 19.5$, high enough to satisfy the condition for homogenization: wavelength over which property transitions is too small compared to the nucleation length. The instability is provoked by an external stress rate, constant in time with a localized peak. (b) Slip rate evolution at each time step is normalized by its peak value. The profile of the diverging slip rate gradually converges to the blow-up solution corresponding to the homogenous (averaged) case, demonstrating supports the results of the present analyses: a fault with a high degree of frictional heterogeneity behaves like a homogenous one.

local, zeroth-order approximation of the variable parameters. In the latter case, the behavior is that of a homogeneous fault with properties being an average over the elasto-frictional length, which samples the rapid variations in this short-wavelength limit. Fig. 5 demonstrates the last point: a diverging slip rate under short wavelengths of property transition gradually attains a blow-up solution corresponding to a completely homogenous fault.

How does one determine if the property variations of a fault lie within either end-member regime, or an intermediate one? If a length scale for variation is posited, or otherwise assumed to exist on some basis, it must then be first compared with an elasto-frictional length. For a fault well represented as slip between elastic half-spaces, we recall that the appropriate length scale is $L_b = \mu D_c / (\sigma b)$. For D_c at the mm-scale implies an elasto-frictional length of the order of 10-100 m for shear modulus, normal stress, and coefficient b of the orders of 10 GPa, 10-100 MPa, and 0.01, respectively. Values of D_c more typically found in laboratory-scale experiments, on the order of 10-100 μm would decrease that estimate by up to two orders of magnitude. For pore-fluid pressure approaching lithostatic, the reduction of the effective normal stress σ to very low values may inflate the estimates of the elasto-frictional length, easily placing a fault in the short-wavelength regime.

APPENDIX A: SLIP RATE AND STATE EVOLUTION

The analysis presented only explicitly considers thin-slab elastic configuration wherein the slip-traction relation is given by

$$\tau_{el}(x, t) = \bar{E}h \frac{\partial^2 \delta(x, t)}{\partial x^2} \quad (\text{A.1})$$

where the elastic modulus $\bar{E} := 2\mu/(1 - \nu)$ and $\bar{E} := \mu$ for mode-II and mode-III sliding respectively. μ and ν are the shear modulus and Poisson's ratio, respectively. However, the results are qualitatively similar for the conventional slip surface within two half-spaces case where the slip-traction relations is given by,

$$\tau_{el}(x, t) = \frac{\bar{\mu}}{2\pi} \int_{L^-}^{L^+} \frac{\partial \delta(\xi, t) / \partial \xi}{\xi - x} d\xi \quad (\text{A.2})$$

where $\bar{\mu} := \mu/(1 - \nu)$ and $\bar{\mu} := \mu$ for in- and anti-plane slip, respectively. The integrand is singular at $\xi = x$ and the integral is evaluated in a Cauchy principal-value sense.

We represent traction-slip relations for both the fault geometries using an operator \mathcal{L} acting on the slip distribution $\delta(x, t)$, that is, $\tau_{el}(x, t) := \mathcal{L}[\delta(x, t)]$. When and where fault has nonzero slip gradient the total shear traction ($\tau_{ex} + \mathcal{L}[\delta(x, t)]$) is equal to the shear strength (τ_s) of the interface. In terms of their rates that equality can be expressed as

$$\frac{\partial \tau_{ex}}{\partial t} + \mathcal{L}[V(x, t)] = \frac{\partial \tau_s}{\partial t} \quad (\text{A.3})$$

where $V(x, t) := \partial \delta / \partial t$ is the slip rate.

We note that as slip attains an unbounded amplitude and the first term in the above equation becomes negligible. Considering a frozen

spatial distribution of fault normal stress $\sigma(x)$ and using time derivative of friction coefficient (equation (5) in the main document), the evolution of the slip rate $V(x, t)$ can be expressed as

$$\frac{\partial V}{\partial t} = V(x, t) \frac{\mathcal{L}[V(x, t)]}{\sigma(x)a(x)} + \frac{b(x)}{a(x)} \frac{V(x, t)^2}{D_c(x)} \left[-\frac{D_c(x)}{V(x, t)} \frac{\partial \theta / \partial t}{\theta(x, t)} \right] \quad (\text{A.4})$$

A scaling analysis suggests the quantity within the bracket should be of order 1 ($\sim O(V^0)$) so that all the terms in the equation are comparable. This motivates to define a surrogate state variable $\Phi(x, t)$, given by,

$$\Phi(x, t) := -\frac{D_c(x)}{V(x, t)} \frac{\partial \theta / \partial t}{\theta(x, t)} \quad (\text{A.5})$$

When aging-law of state evolution is considered the above definition assumes the form

$$\Phi(x, t) = 1 - \frac{D_c(x)}{V(x, t)\theta(x, t)} \quad (\text{A.6})$$

With this definition, Φ can be interpreted as a measure of distance from steady-state sliding: $\Phi = 0$ for steady-state sliding ($V\theta/D_c = 1$) and $\Phi = 1$ when state of the slip is far from steady-state ($V\theta/D_c \gg 1$). The coupled system of quasistatic slip acceleration and evolution of $\Phi(x, t)$ with time, is given by

$$\frac{\partial V}{\partial t} = V(x, t) \frac{\mathcal{L}[V(x, t)]}{\sigma(x)a(x)} + \frac{b(x)}{a(x)} \frac{V(x, t)^2}{D_c(x)} \Phi(x, t) \quad (\text{A.7a})$$

$$\frac{\partial \Phi}{\partial t} = [1 - \Phi(x, t)] \left[\frac{\mathcal{L}[V(x, t)]}{\sigma(x)a(x)} + \left(\frac{b(x)}{a(x)} - 1 \right) \frac{V(x, t)}{D_c(x)} \Phi(x, t) \right] \quad (\text{A.7b})$$

The functional forms $\mathcal{R}[V(x, t), \Phi(x, t)]$ and $\mathcal{S}[V(x, t), \Phi(x, t)]$, in the system of equations (9) of the main document, are respectively given by the right sides of (A.7a) and (A.7b).

APPENDIX B: BLOW-UP SOLUTIONS AND THEIR ATTAINABILITY

Previous studies Viesca (2016b,a); Ray & Viesca (2017) showed that system of equations (A.7) has a solution of the form

$$V(x, t) = \frac{D_c(x)}{t_f} \mathcal{W}(x) \quad \text{and} \quad \Phi(x, s) = \mathcal{P}(x) \quad (\text{B.1})$$

where the $t_f = t_{in} - t$ is the time remaining to instability and t_{in} as time of instability. The profile $\mathcal{W}(x)$, referred to as blow-up solution, and its support on the fault are to be solved for. The profile $\mathcal{P}(x)$ is obtained from $\mathcal{W}(x)$ and shows the proximity of the instability from the steady state slip. On substituting above in the evolution equations (A.7) and choosing thin slab elastic configuration (A.1), we get,

$$\frac{\bar{E}h D_c}{\sigma(x)a(x)} \frac{d^2 \mathcal{W}}{dx^2} + \frac{b(x)}{a(x)} \mathcal{W}(x) \mathcal{P}(x) = 1 \quad (\text{B.2a})$$

$$[1 - \mathcal{P}(x)][1 - \mathcal{W}(x)\mathcal{P}(x)] = 0 \quad (\text{B.2b})$$

We recall that Φ by its definition (A.6) is the measure of proximity to steady state sliding and lies between 0 (steady state) and 1 (far above and below steady state); and hence, the $\mathcal{P}(x) = 1$ or $\mathcal{W}\mathcal{P} = 1$, respectively, for $\mathcal{W}(x)$ below or above unity Viesca (2016a,b); Ray & Viesca (2017).

B1 Stability analysis of the blow-up solutions

The blow-up solutions, $\mathcal{W}(x)$, and its support on the fault, $2L$, are straightforward to be solved for; however, Ray & Viesca (2017) showed existence of multiple solutions under nonuniform parameter distributions. This naturally raises the question of attainability of a particular blow-up solution; which, in turn, equivalent to asking if a preferential evolution of (A.7) is possible when provoked by an external or initial condition.

In order to address if a particular blow-up solution is realizable, we perturb the blow-up solution $\mathcal{W}(x)$ by a small function $\omega(x)$, and analyze when the perturbed velocity profile, given by,

$$V(x, t) = \frac{D_c(x)}{t_f} [\mathcal{W}(x) + \omega(x)(t_f/t_o)^{-\lambda}] \quad (\text{B.3})$$

might converge to or diverge from the spatial profile $\mathcal{W}(x)$. That is, we analyze when and where on the fault the perturbation $\omega(x)$ could grow or decay as $t_f \rightarrow 0$, which is dictated by the sign of $\text{Re}(\lambda_{max})$. Likewise, we also consider whether a perturbation to the state variable in the form

$$\Phi(x, t) = \mathcal{P}(x) + \phi(x)(t_f/t_o)^{-\lambda} \quad (\text{B.4})$$

might grow or shrink as $t_f \rightarrow 0$.

On substituting the above perturbations (B.3, B.4) in (A.7) permits to consider the functions $\omega(x)$ and $\phi(x)$ and the scalar λ as solutions to an eigenvalue problem, given by,

$$\lambda \begin{bmatrix} \omega(x) \\ \phi(x) \end{bmatrix} = \begin{bmatrix} A_{11} & A_{12} \\ A_{21} & A_{22} \end{bmatrix} \begin{bmatrix} \omega(x) \\ \phi(x) \end{bmatrix} \quad (\text{B.5})$$

where the terms inside the matrix, for the thin-slab elastic configuration and with heterogeneity only in the parameter $a(x)$, are given by,

$$\begin{aligned} A_{11} &= \frac{\mathcal{W}(x)}{a(x)/b} \left[L_{bh}^2 \frac{d^2}{dx^2} + \mathcal{P}(x) \right] \\ A_{12} &= \frac{\mathcal{W}(x)^2}{a(x)/b} \\ A_{21} &= \frac{1 - \mathcal{P}(x)}{a(x)/b} \left[L_{bh}^2 \frac{d^2}{dx^2} + (1 - a(x)/b) \mathcal{P}(x) \right] \\ A_{22} &= \frac{1 - a(x)/b}{a(x)/b} [1 - \mathcal{P}(x)] \mathcal{W}(x) - [1 - \mathcal{W}(x) \mathcal{P}(x)] \end{aligned}$$

The blow-up solution $\mathcal{W}(x)$ is attainable when the maximum eigenvalue, $\lambda = \lambda_{max}$, has negative real and are referred to as stable solutions. In Figures 3 and 4 in the main document we plot the maximum eigenvalue, $\lambda = \lambda_{max}$, that determines the attainability of the blow-up solutions $\mathcal{W}(x)$ in (B.1).

We note that the above eigenvalue problem is equivalent to that of the linear stability analysis of the fixed point solutions in Viesca (2016b,a); Ray & Viesca (2017). Considering solutions for which $\mathcal{P}(x) = 1$ in above allows us to focus on a reduced version of the eigenvalue problem wherein only the eigenmode $\omega(x)$ needs to be analyzed. A suitable rearrangement of the terms allow us to re-express the eigen-equation in the simple form

$$L_{bh}^2 \frac{d^2 \omega}{dx^2} + \omega(x) = \lambda \left[\frac{a(x)/b}{\mathcal{W}(x)} \right] \omega(x) \quad (\text{B.6})$$

B2 Spatial symmetry eigenmode

Here, we re-highlight the existence of spatial-symmetry eigenmode for its relevance to the consideration of heterogeneous distributions of properties and its apparent connection with the observed stability reversals of blow-up solutions and homogenization.

We look for the eigenmode and eigenvalue indicating that a blow-up solution remains invariant when translated along the fault Ray & Viesca (2017). Presuming that shifting the origin of the blow-up solution, by a small quantity ϵ , has no bearing on the form of the diverging slip rate (B.1), we may write

$$V(x, t) = \frac{D_c}{t_f} \mathcal{W}(x + \epsilon)$$

which may be expanded to first-order in the perturbation as

$$V(x, t) = \frac{D_c}{t_f} [\mathcal{W}(x) + \epsilon \mathcal{W}'(x)]$$

Comparing this last result with equation (B.3), we see that translational symmetry corresponds to the existence of an eigenmode and eigenvalue satisfying

$$\omega(x) = \mathcal{W}'(x) \quad \text{with} \quad \lambda = 0 \quad (\text{B.7})$$

APPENDIX C: BLOW-UP SOLUTIONS UNDER VARIATIONS OF $a(x)$ WITH INTEGER WAVENUMBER

We recall that in Figure 3 of the main text, the blow-up solutions at the maximum and minimum of the $a(x)/b$ distribution exchange their stability at integer wavenumbers $\kappa \neq 1$. In that figure, the stability curves (λ_{max} vs. κ) for the solutions at the extrema of $a(x)/b$ cross $\lambda_{max} = 0$ simultaneously. This is a signature of a transcritical bifurcation of the fixed-point solutions. Here, we show how the stability reversals may be anticipated to occur at integer wavenumbers, if anywhere. Furthermore, we show how a translational symmetry mode is retrieved in the limit of large values of κ , the limit for which we found homogenization to be appropriate. We consider the simple periodic variation of the parameter $a(x)/b = a_0 + a_1 \cos(\kappa x/L_{bh})$, with uniform σ and D_c . For solutions with $\mathcal{P}(x) = 1$, (B.2a) reduces to

$$L_{bh}^2 \frac{d^2 \mathcal{W}}{dx^2} + \mathcal{W}(x) = a_0 + a_1 \cos(\kappa x/L_{bh}) \quad (\text{C.1})$$

with the boundary conditions $\mathcal{W}(\pm L) = 0$ and $\mathcal{W}'(\pm L) = 0$ determining both $\mathcal{W}(x)$ and L/L_{bh} . The blow-up solutions corresponding to the maximum and minimum of $a(x)/b$ are obtained by switching the algebraic sign of a_1 . For integer wavenumbers, $\kappa = n \neq 1$, the solution to (C.1) is

$$\mathcal{W}(x) = a_0 [1 + \cos(x/L_{bh})] + \frac{a_1}{1 - n^2} [\cos(x/L_{bh}) + (-1)^n \cos(nx/L_{bh})], \quad L/L_{bh} = \pi \quad (\text{C.2})$$

We note that the value of L/L_{bh} is equal to that for the homogeneous problem ($a_1 = 0$) for all $\kappa = n$. We also note that at large n the second term vanishes as n^{-2} , leaving only the solution to the homogeneous problem.

We may now proceed to find the eigenmodes associated with $\lambda = 0$ at integer κ following the linear stability analysis of these blow-up solutions. Specifically, we substitute $\lambda = 0$ in the reduced eigenvalue problem (B.6) and solve for the corresponding eigenfunction which satisfies

$$\frac{L_{bh}^2}{L^2} \frac{d^2\omega}{d\tilde{x}^2} + \omega(\tilde{x}) = 0 \quad (\text{C.3})$$

where we have performed a change of the independent variable $\tilde{x} = x/L$. Given that $L/L_{bh} = \pi$ at integer κ , the general solution is a linear combination of $\sin(\pi\tilde{x})$ and $\cos(\pi\tilde{x})$. Imposing the boundary conditions $\omega(\tilde{x} = \pm 1) = 0$ eliminates the latter function and leaves

$$\omega(x) = \sin(\pi x/L) \quad \text{with } \lambda = 0 \quad \text{for } \kappa = n = 2, 3, 4, \dots \quad (\text{C.4})$$

Re-examining (C.2), we see that

$$\lim_{n \rightarrow \infty} \mathcal{W}'(x) = -a_0 \sin(x/L_{bh}) = -a_0 \sin(\pi x/L) \quad (\text{C.5})$$

and upon finding that this result is, to within an arbitrary pre-factor, equal to the eigenmode (C.4), we find that we retrieve the translational symmetry mode condition (B.7) in the limit of large κ . Thus we find that, in the highly heterogeneous limit of large κ , the blow-up solutions regain the translational invariance that would be expected for a homogeneous fault.

ACKNOWLEDGMENTS

The authors gratefully acknowledge support from NSF via grants EAR-1344993 and EAR-1653382 and from the Southern California Earthquake Center (SCEC). SCEC is funded by NSF Cooperative Agreement EAR-1600087 and USGS Cooperative Agreement G17AC00047. The authors are grateful to the two anonymous reviewers for their comments.

References

- Aldam, M., Weikamp, M., Spatschek, R., Brener, E. A., & Bouchbinder, E., 2017. Critical Nucleation Length for Accelerating Frictional Slip, *Geophys. Res. Lett.*, **44**(22), 11,390–11,398.
- Ampuero, J.-P., Ripperger, J., & Mai, P. M., 2006. Properties of dynamic earthquake ruptures with heterogeneous stress drop, in *Radiated Energy and the Physics of Earthquakes*, pp. 255–261, eds McGarr, A., Abercrombie, R. E., Kanamori, H., & Di Toro, G., Geophysical Monograph Series 170, American Geophysical Union, Washington, D. C.
- Aochi, H. & Ide, S., 2004. Numerical study on multi-scaling earthquake rupture, *Geophysical Research Letters*, **31**(2).
- Bar-Sinai, Y., Brener, E. A., & Bouchbinder, E., 2012. Slow rupture of frictional interfaces, *Geophys. Res. Lett.*, **39**(3).
- Barenblatt, G. I., 1996. *Scaling, self-similarity, and intermediate asymptotics: dimensional analysis and intermediate asymptotics*, vol. 14, Cambridge University Press.
- Bayart, E., Svetlizky, I., & Fineberg, J., 2015. Fracture mechanics determine the lengths of interface ruptures that mediate frictional motion, *Nat. Phys.*, pp. 1–6.
- Bilby, B. & Eshelby, J., 1968. Fracture, an advanced treatise, in *Microscopic and Macroscopic Fundamentals*, vol. 1, p. 29, Academic Press New York and London.
- Blanpied, M. L., Lockner, D. A., & Byerlee, J. D., 1991. Fault stability inferred from granite sliding experiments at hydrothermal conditions, *Geophys. Res. Lett.*, **18**(4), 609–612.
- Dieterich, J. H., 1978. Time-dependent friction and the mechanics of stick-slip, *Pure Appl. Geophys.*, **116**(4), 790–806.
- Dieterich, J. H., 1981. Constitutive properties of faults with simulated gouge, *Mechanical behavior of crustal rocks: the Handin volume*, **24**, 103–120.
- Dieterich, J. H., 1992. Earthquake nucleation on faults with rate-and state-dependent strength, *Tectonophysics*, **211**(1), 115–134.
- Dublanchet, P., 2017. The dynamics of earthquake precursors controlled by effective friction, *Geophysical Journal International*, **212**(2), 853–871.
- Goldsby, D. L. & Tullis, T. E., 2011. Flash Heating Leads to Low Frictional Strength of Crustal Rocks at Earthquake Slip Rates, *Science*, **334**(6053), 216–218.
- Ide, S. & Aochi, H., 2005a. Earthquakes as multiscale dynamic ruptures with heterogeneous fracture surface energy, *J. Geophys. Res.*, **110**(B11), 3575–10.
- Ide, S. & Aochi, H., 2005b. Earthquakes as multiscale dynamic ruptures with heterogeneous fracture surface energy, *Journal of Geophysical Research: Solid Earth*, **110**(B11).
- Kammer, D. S., Radiguet, M., Ampuero, J.-P., & Molinari, J.-F., 2015. Linear Elastic Fracture Mechanics Predicts the Propagation Distance of Frictional Slip, *Tribology Letters*, **57**(3).

- Ke, C. Y., McLaskey, G. C., & Kammer, D. S., 2018. Rupture Termination in Laboratory-Generated Earthquakes, *Geophys. Res. Lett.*, **308**, 681–9.
- Lipovsky, B. P. & Dunham, E. M., 2017. Slow-slip events on the Whillans Ice Plain, Antarctica, described using rate-and-state friction as an ice stream sliding law, *J. Geophys. Res. Earth Surf.*, **122**(4), 973–1003.
- Luo, Y. & Liu, Z., 2019. Rate-and-state model casts new insight into episodic tremor and slow-slip variability in Cascadia, *Geophysical Research Letters*.
- Puzrin, A. M. & Germanovich, L. N., 2005. The growth of shear bands in the catastrophic failure of soils, *P. Roy. Soc. A.*, **461**(2056), 1199–1228.
- Ray, S. & Viesca, R. C., 2017. Earthquake Nucleation on Faults With Heterogeneous Frictional Properties, Normal Stress, *J. Geophys. Res.*, **122**(10), 8214–8240.
- Rice, J. R., 1968. A path independent integral and the approximate analysis of strain concentration by notches and cracks, *Journal of applied mechanics*, **35**(2), 379–386.
- Rice, J. R., 2006. Heating and weakening of faults during earthquake slip, *J. Geophys. Res.*, **111**, B05311.
- Rice, J. R. & Ruina, A. L., 1983. Stability of steady frictional slipping, *J. Appl. Mech.*, **50**, 343–349.
- Rice, J. R., Lapusta, N., & Ranjith, K., 2001. Rate and state dependent friction and the stability of sliding between elastically deformable solids, *J. Mech Phys. Solids*, **49**(9), 1865–1898.
- Ripperger, J., Ampuero, J.-P., Mai, P. M., & Giardini, D., 2007. Earthquake source characteristics from dynamic rupture with constrained stochastic fault stress, *J. Geophys. Res.*, **112**(B4).
- Rubin, A. M. & Ampuero, J.-P., 2005. Earthquake nucleation on (aging) rate and state faults, *J. Geophys. Res.*, **110**, B11312.
- Rubin, A. M., Gillard, D., & Got, J. L., 1999. Streaks of microearthquakes along creeping faults, *Nature*, **400**(6745), 635–641.
- Ruina, A., 1983. Slip instability and state variable friction laws, *J. Geophys. Res.*, **88**(B12), 10359–10370.
- Stesky, R. M., 1975. *The mechanical behavior of faulted rock at high temperature and pressure.*, Ph.D. thesis, Massachusetts Institute of Technology.
- Tse, S. T. & Rice, J. R., 1986. Crustal Earthquake Instability in Relation to the Depth Variation of Frictional Slip Properties, *J. Geophys. Res.*, **91**, 9452–9472.
- Uenishi, K. & Rice, J. R., 2003. Universal nucleation length for slip-weakening rupture instability under nonuniform fault loading, *Journal of Geophysical Research: Solid Earth*, **108**(B1).
- Viesca, R. C., 2016a. Stable and unstable development of an interfacial sliding instability, *Phys. Rev. E*, **93**(6), 060202(R).
- Viesca, R. C., 2016b. Self-similar slip instability on interfaces with rate- and state-dependent friction, *Proceedings of the Royal Society A: Mathematical, Physical and Engineering Science*, **472**(2192), 20160254.
- Waldhauser, F., Ellsworth, W. L., Schaff, D. P., & Cole, A., 2004. Streaks, multiplets, and holes: High-resolution spatio-temporal behavior of Parkfield seismicity, *Geophys. Res. Lett.*, **31**(18), 619–5.